

# Open Research Online

---

The Open University's repository of research publications and other research outputs

## Feasibility studies for hydrogen reduction of ilmenite in a static system for use as an ISRU demonstration on the lunar surface

### Journal Item

#### How to cite:

Sargeant, H. M.; Abernethy, F. A. J.; Anand, M.; Barber, S. J.; Landsberg, P.; Sheridan, S.; Wright, I. and Morse, A. (2020). Feasibility studies for hydrogen reduction of ilmenite in a static system for use as an ISRU demonstration on the lunar surface. *Planetary and Space Science*, 180, article no. 104759.

For guidance on citations see [FAQs](#).

© 2019 Elsevier Ltd.

Version: Accepted Manuscript

Link(s) to article on publisher's website:

<http://dx.doi.org/doi:10.1016/j.pss.2019.104759>

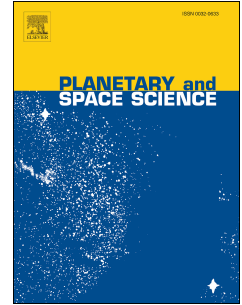
---

Copyright and Moral Rights for the articles on this site are retained by the individual authors and/or other copyright owners. For more information on Open Research Online's data [policy](#) on reuse of materials please consult the policies page.

---

[oro.open.ac.uk](http://oro.open.ac.uk)

# Journal Pre-proof



Feasibility studies for hydrogen reduction of ilmenite in a static system for use as an ISRU demonstration on the lunar surface

H.M. Sargeant, F.A.J. Abernethy, M. Anand, S.J. Barber, P. Landsberg, S. Sheridan, I. Wright, A. Morse

PII: S0032-0633(18)30400-8

DOI: <https://doi.org/10.1016/j.pss.2019.104759>

Reference: PSS 104759

To appear in: *Planetary and Space Science*

Received Date: 6 November 2018

Revised Date: 11 September 2019

Accepted Date: 26 September 2019

Please cite this article as: Sargeant, H.M., Abernethy, F.A.J., Anand, M., Barber, S.J., Landsberg, P., Sheridan, S., Wright, I., Morse, A., Feasibility studies for hydrogen reduction of ilmenite in a static system for use as an ISRU demonstration on the lunar surface, *Planetary and Space Science* (2019), doi: <https://doi.org/10.1016/j.pss.2019.104759>.

This is a PDF file of an article that has undergone enhancements after acceptance, such as the addition of a cover page and metadata, and formatting for readability, but it is not yet the definitive version of record. This version will undergo additional copyediting, typesetting and review before it is published in its final form, but we are providing this version to give early visibility of the article. Please note that, during the production process, errors may be discovered which could affect the content, and all legal disclaimers that apply to the journal pertain.

© 2019 Published by Elsevier Ltd.

1 **Feasibility Studies for Hydrogen Reduction of Ilmenite in a Static System for use as an**  
2 **ISRU Demonstration on the Lunar Surface**

3 **H.M. Sargeant<sup>1</sup>, F.A.J. Abernethy<sup>1</sup>, M. Anand<sup>1,2</sup>, S.J Barber<sup>1</sup>, P. Landsberg<sup>1</sup>, S.**  
4 **Sheridan<sup>1</sup>, I. Wright<sup>1</sup>, A. Morse<sup>1</sup>.**

5 <sup>1</sup>School of Physical Sciences, The Open University, Milton Keynes MK7 6AA, UK.

6 <sup>2</sup>Department of Earth Sciences, The Natural History Museum, London, SW7 5BD, UK.

7 Corresponding author: Hannah Sargeant ([hannah.sargeant@open.ac.uk](mailto:hannah.sargeant@open.ac.uk))

8 **Abstract**

9 The ESA-ROSCOSMOS mission, Luna-27, scheduled for launch in 2023,  
10 includes a payload known as PROSPECT that is intended for sampling the polar lunar  
11 regolith through drilling, with subsequent analyses of the retrieved material. One of the  
12 aims of the analytical module, ProSPA, which is being developed at The Open  
13 University, is to identify and quantify the volatiles present in the extracted sample that  
14 are released by heating from ambient up to 1000 °C and analyzed by the mass  
15 spectrometers to assess their potential for in-situ resource utilization. The ProSPA  
16 design also includes a provision to test the extraction of water (and its associated  
17 oxygen) from lunar regolith by hydrogen reduction. Previous attempts at such  
18 extractions generally utilize a flow of hydrogen gas through the feedstock to efficiently  
19 extract water. However, in ProSPA, samples would be processed in a static mode,  
20 which leads to concerns that the reaction may be suppressed by inefficient removal of  
21 water vapor above the regolith. A first order theoretical assessment of the diffusion of

22 gases in such a system was performed and suggested that water can diffuse through  
23 the system at an acceptable rate and be collected upon a cold finger thus enabling the  
24 reaction to proceed. Proof of concept experiments were successfully performed with a  
25 ProSPA breadboard using ilmenite samples up to ~45 mg heated at 900 °C for 60  
26 minutes. Subsequent heating of the cold finger, in vacuum, released  $17\pm 1$   $\mu\text{mol}$  water  
27 from a  $44.7\pm 0.5$  mg sample, equating to a calculated yield of  $0.6\pm 0.1$  wt. % oxygen, and  
28 a reduction extent of  $5.8\pm 0.4$  %. A sample of mass  $11.2\pm 0.5$  mg had the greatest  
29 calculated yield of  $1.4\pm 0.2$  wt. % oxygen, and this equates to a reduction extent of  
30  $12.9\pm 1.5$  %. SEM analyses of cross-sections of grains showed evidence of a reduction  
31 reaction inside the ilmenite grains with some showing greater reduction than others,  
32 indicating the reaction is limited by furnace dimensions, reaction kinetics and geometry.  
33 The results suggest that the ProSPA ISRU experiment should be capable of producing  
34 water, and therefore oxygen, by hydrogen reduction of ilmenite, ultimately this could be  
35 a viable technique for producing oxygen from ilmenite-containing lunar regolith with  
36 ProSPA.

37 **Keywords**

38 #ISRU #Ilmenite #Hydrogen Reduction #PROSPECT #ProSPA #Moon

## 39 **Highlights**

- 40 • Hydrogen gas can reduce ilmenite in a ProSPA-type system to produce water
- 41 • Water can be condensed and released for quantification using a cold finger
- 42 • The ProSPA ISRU experiment is a useful prospecting technique

## 43 **1 Introduction**

44 In Situ Resource Utilization (ISRU) is the concept of harvesting local resources,  
45 resulting in space exploration missions that would ultimately be more cost-effective than  
46 those solely reliant on the transport of resources from the Earth. Although theoretical  
47 ISRU studies have been undertaken from as early as 1979 (Rao et al., 1979), more  
48 attention has been paid to laboratory and field studies in the last decade (e.g. Sanders  
49 & Larson, 2012) as such technologies could enable future long term exploration  
50 missions to the Moon and Mars (ESA, 2015; ISECG, 2018).

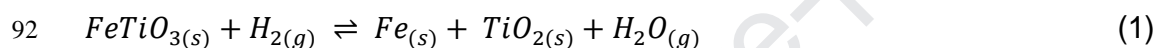
51 The ambition to develop a long-term sustainable presence in space has spurred the  
52 proposal, study and development of a number of ISRU demonstration and resource  
53 prospecting instruments. Examples of such technologies include ROxygen and PILOT  
54 (Pre-cursor ISRU Lunar Oxygen Testbed) which both perform hydrogen reduction of  
55 regolith with yields of 1-2 wt.% oxygen production from regolith. The RESOLVE  
56 (Regolith and Environmental Science and Oxygen and Lunar Volatile Extraction)  
57 instrument looks for volatiles in permanently shadowed regions as well as performing  
58 hydrogen reduction of regolith (Sanders and Larson, 2011, 2012). The Mars Oxygen In-  
59 Situ Resource Utilization Experiment, MOXIE, is a payload on the Mars 2020 rover

60 which will extract oxygen from the Martian atmosphere (Meyen et al., 2016). The  
61 European Space Agency (ESA) has committed to performing a lunar ISRU  
62 demonstration mission by 2025 (ESA, 2018). Such a mission will build on findings  
63 highlighted at the European-wide ISRU workshop (Anand et al., 2018), and research  
64 performed in European institutions (e.g. Denk, 2018; Lomax et al., 2019). The primary  
65 ISRU goals of these ventures are the production of water and/or its components from  
66 local resources. As a complement to the ESA 2025 mission, an instrument called  
67 ProSPA (PROSPECT Sample Processing and Analysis) is being developed at The  
68 Open University as part of ESA's Package for Resource Observation and in situ  
69 Prospecting for Exploration, Commercial Exploitation and Transportation (PROSPECT)  
70 (Barber et al., 2017) on-board the Luna-27 mission. As part of the Luna-27 mission,  
71 currently aimed for a launch in 2025, PROSPECT aims to identify and quantify volatiles  
72 at a high-latitude region of the Moon. The volatiles in question will be released by  
73 heating samples of regolith to temperatures of up to 1000 °C. In addition to determining  
74 the lunar volatile inventory, ProSPA will perform a proof-of-principle ISRU water/oxygen  
75 extraction experiment on the lunar surface.

76 Numerous methods have been hypothesized for extracting oxygen from the lunar  
77 regolith which fall into three main categories (Taylor & Carrier, 1993); solid/gas  
78 interaction, silicate/oxide melt, and pyrolysis. Each process has advantages and  
79 disadvantages with respect to the feedstock used, the resupply mass of any required  
80 materials (i.e. reactants or hardware), the complexity of the process, and the energy  
81 required. The titanium- and iron-bearing mineral ilmenite ( $\text{FeTiO}_3$ ) is found in lunar  
82 basalts in varying concentrations (Papike et al., 1991), and has been proposed as a

83 potential source of oxygen (Taylor and Carrier, 1993). Reduction by hydrogen has long  
 84 been considered the optimum method of extracting oxygen from ilmenite in lunar  
 85 samples (Gibson & Knudsen, 1985). The main benefits being that hydrogen (of solar  
 86 wind origin) can be extracted from the lunar regolith which reduces the resupply mass  
 87 from Earth, its relatively low operating temperatures at 700-1000°C (Taylor & Carrier,  
 88 1993), and its simple operational process (Christiansen et al., 1988; Zhao & Shadman,  
 89 1993).

90 Reduction of ilmenite by hydrogen gas is an equilibrium reaction (1), with the  
 91 physical state of each reactant and product denoted as (s) solid or (g) gas:



93 In order to maintain the reduction, the water vapor produced by the reaction needs to be  
 94 constantly removed from the gas phase, e.g. via a flowing gas to a condenser. Taylor et  
 95 al. (1993) suggested that the partial pressure of H<sub>2</sub>O vapor at the reaction site must  
 96 remain below 10 % for the reaction to continue, whilst work by Altenberg et al. (1993)  
 97 suggested that up to 30 % partial pressure of H<sub>2</sub>O is permissible for the reaction to  
 98 continue when operating in low pressures of 1-100 mbar at 900 °C.

99 Previous studies, aimed specifically at ISRU capabilities, have used gas and/or  
 100 vibrational fluidization techniques which improves mixing of the reactants and removal  
 101 of the produced water (Christiansen et al., 1998; Gibson & Knudsen, 1985; Linne et al.,  
 102 2009, 2012). A Significant limitation of the ProSPA system is that it is a static (non-  
 103 flowing) and stationary (no fluidized bed or rotating drum) system, that utilizes a static  
 104 volume of hydrogen gas. Instead, a cold trap is used to remove any water that is

105 produced, as suggested by Williams et al. (1979) and Williams & Mullins (1983), and  
106 maintains a sufficiently low level partial pressure of water at the reaction site.

107 The ProSPA system adopts heritage from Ptolemy (Wright et al., 2007) and the  
108 Gas Analysis Package, GAP (Talboys et al., 2009), and is primarily designed for the  
109 characterization of volatiles, and isotope analysis. ProSPA, therefore, did not originate  
110 with an ISRU focus and as a consequence has a non-ideal configuration for such  
111 experiments. The purpose of the present work is to investigate the feasibility of  
112 performing an ISRU demonstration with the ProSPA flight instrument on the lunar  
113 surface. The ProSPA analytical laboratory contains much of the requisite hardware – for  
114 instance furnaces capable of heating the sample to 1000 °C, hydrogen gas supply, a  
115 gas control system, pressure sensors, a cold finger for collecting volatiles, and two  
116 mass spectrometers to monitor the reaction (Barber et al., 2018). A static system  
117 simplifies the ProSPA design, avoiding the need for complex reactors, and gas  
118 circulation system. This work therefore concerns the evaluation of the feasibility of  
119 ProSPA to demonstrate hydrogen reduction of ilmenite grains to produce water in a  
120 static system.

121 Of the iron oxide bearing minerals available on the Moon, ilmenite will most  
122 readily reduce (Allen et al., 1994), and therefore produce the highest yields in a given  
123 time when reduced with hydrogen. Although ilmenite is thought to be found in relatively  
124 high concentrations of up to 20 % by volume in mare regions (Warner et al. 1978,  
125 Chambers et al. 1995, Papike et al. 1998, Hallis et al. 2014), highland regions, such as  
126 the high latitude regions where Luna-27 is expected to land, can contain <1 % by  
127 volume (Taylor et al., 2010). To avoid the possibility of little to no measurable yield, pure



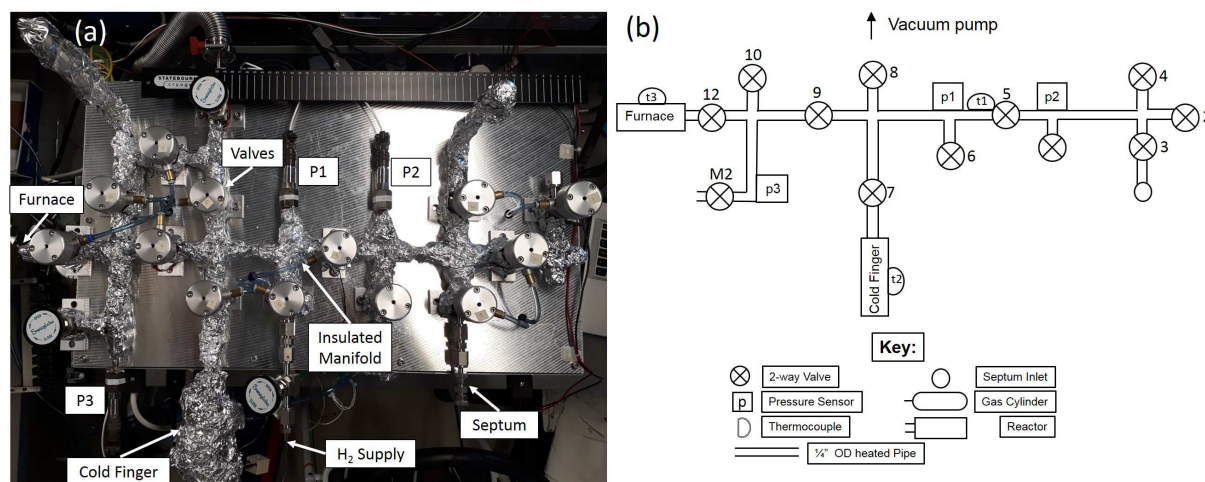
128 ilmenite was chosen for this initial study to ensure the system is first capable of reducing  
129 the mineral. Lunar soil and simulants at this stage of the study would also complicate  
130 results as a consequence of their complex mineralogies which could cause secondary  
131 reactions to take place. As well as determining whether ProSPA can be used to perform  
132 ilmenite reduction reactions, this study aims to determine how the quantity of ilmenite  
133 present affects the measured yield. This will ultimately enable ProSPA to quantify the  
134 water that can be produced from ilmenite-bearing lunar soil.

## 135 **2 Materials and Methods**

### 136 **2.1 System design**

137 In terms of space instrument design, a so-called breadboard model is one that  
138 replicates the intended functionality without recourse to using highly specialized space-  
139 qualified components, and is largely free of the overall mass/volume/power  
140 consumption constraints imposed on flight hardware. One of the breadboard models of  
141 the ProSPA gas processing system, known as the Benchtop Demonstration Model  
142 (BDM) is shown in Fig. 1(a). The BDM is based on the overall ProSPA system diagram  
143 (Barber et al., 2017). A schematic diagram of the section of the BDM used for  
144 evaluating the ISRU experiment is shown in Fig. 1 (b)

145



146

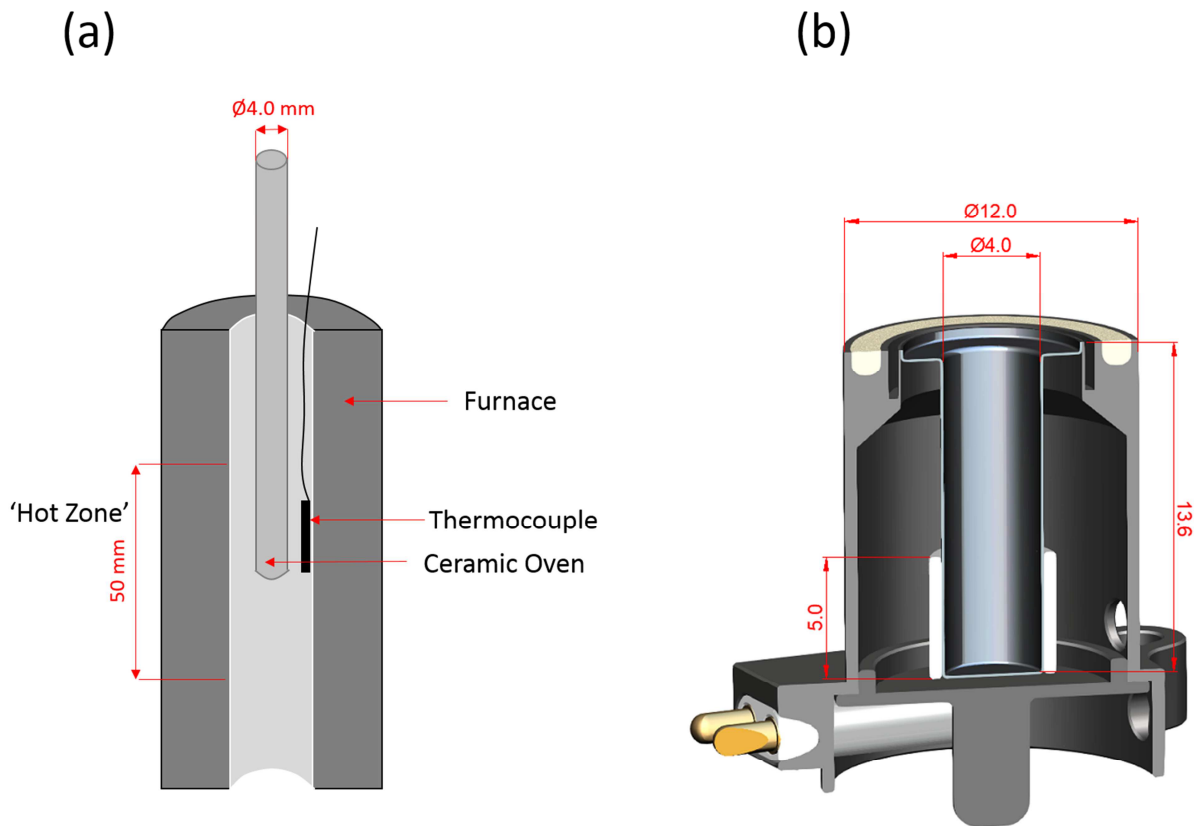
147

148 *Fig. 1 (a) Labelled BDM image (b) BDM system diagram.*

149 The purpose of the BDM is to be a testbed for ProSPA flight components and science  
 150 experiments. The details of the BDM design are described in Supplementary Material  
 151 (S1). It contains mainly commercial off the shelf parts connected together in a similar  
 152 configuration to that of the intended flight design.

153 The sample 'oven' consists of a 200 mm long ceramic tube (LEWVAC, 99.7% Al<sub>2</sub>O<sub>3</sub>) of  
 154 4 mm internal diameter (ID) and 6 mm outer diameter (OD). It is placed inside a  
 155 resistance-element furnace capable of reaching temperatures of 1200 °C (Fig. 2a). The  
 156 ProSPA flight ovens (Fig. 2b) have internal dimensions of 4 mm ID and 13.6 mm depth  
 157 and are designed to hold a sample mass of ~50 mg. As such the BDM oven  
 158 arrangement replicates the flight oven's 4 mm internal diameter, ensuring the sample is  
 159 held in the same shape as would be in the ProSPA oven. Although the hot zone is  
 160 significantly greater in the BDM design, both the BDM and ProSPA oven hot zones are  
 161 sufficient to uniformly heat a 50 mg ilmenite sample.

162 The BDM cold finger temperature was controlled by an automated supply of nitrogen  
163 gas cooled by passing through a liquid nitrogen dewar, in combination with an electric  
164 heating wire. Hydrogen gas (Laborgase, 99.999% purity) was supplied from a 12 L  
165 lecture bottle. The pressure of gas in the system was measured by silicon on insulator  
166 (SOI) diaphragm pressure sensors (Kulite, ETL-375CO-1.1BARA), and the manifold  
167 was heated by heater tape to 115 °C in order to prevent water vapor condensing when  
168 measuring vapor gas pressure. The valves and pressure sensors were not directly  
169 heated in order to avoid exceeding their permissible temperature range; they therefore  
170 operated at ~65 °C and 35 °C, respectively. Internal volumes of the BDM pipework were  
171 calibrated by expanding dry nitrogen gas from a 2 L volume incrementally into various  
172 sections of the extraction system. With the initial volume and pressure known, and with  
173 temperature remaining constant throughout the expansion, the change in pressure  
174 recorded during each expansion correlates to a change in volume.



175

176 *Fig. 2 (a) Furnace heater design, cross section. (b) ProSPA oven design CAD drawing.*

177 *The samples are deposited by the drill into the 4 mm ID oven and heated by an*  
178 *electrical resistance element.*

## 179 **2.2 Ilmenite Feedstock**

180 The ilmenite feedstock used in this work was supplied by the ESA European Astronaut  
181 Centre (EAC) in Cologne, Germany. According to mineral analyses by EAC, it is  
182 dominated by modal ilmenite (95 %) with some minor modal impurities comprising of  
183 silica (1-2 %), quartz (1-2 %), and other phases (1-2 %). A representative aliquot of  
184 ilmenite feedstock was used for grain-size distribution analyses using a Nikon SMZ1500  
185 microscope and images taken with infinity capture software at a magnification of 10x  
186 before being analyzed in Image J open source software. Assuming that the grains are

187 spherical, the grain diameters were determined to be between 80 and 260  $\mu\text{m}$  with an  
188 average diameter of 170  $\mu\text{m}$  across the randomly selected grains analyzed. Although  
189 still relatively coarse compared to lunar soil, it was determined to be a suitable proxy for  
190 ilmenite that is found in lunar soils as for example in an Apollo 17 soil, ilmenite was  
191 found to have grain sizes of 45-500  $\mu\text{m}$  (McKay et al., 1991). To remain representative  
192 of ProSPA capabilities, ilmenite samples of 45 mg (0.3 mmol) were used in the following  
193 ilmenite reduction studies.

194

### 195 **2.3 Thermogravimetric – Mass Spectrometry (TG-MS) Analysis**

196 TG-MS analyses were performed using a Netzsch Jupiter STA (Simultaneous Thermo-  
197 Analyzer) 449C, coupled to a Hiden HPR-20 quadrupole mass spectrometer via a  
198 stainless steel crimped capillary inlet.

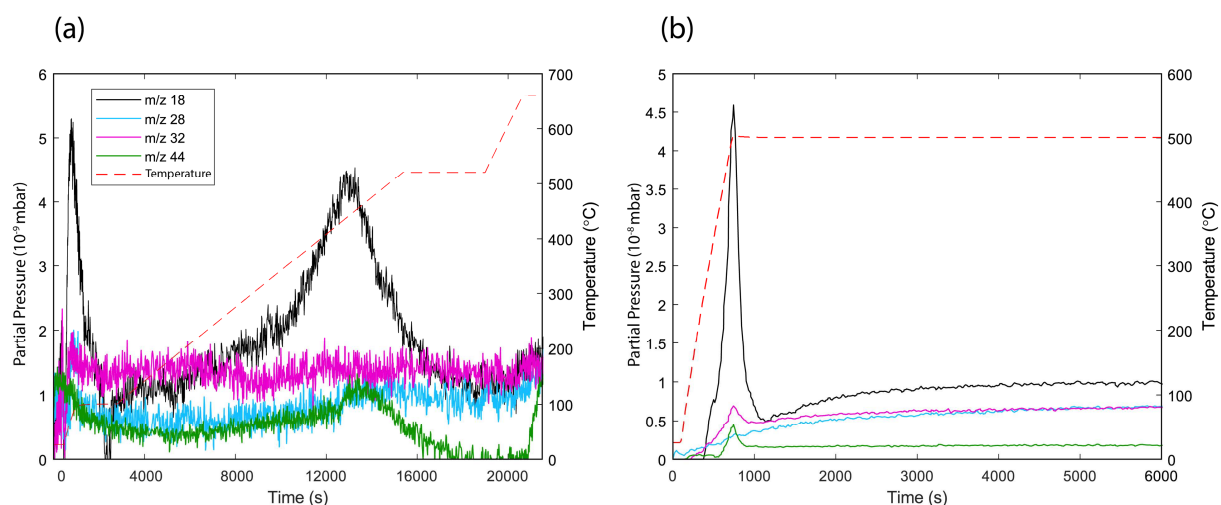
199 To determine the temperature of bake-out, a 134.9 mg ilmenite sample was  
200 heated using a 3-stage ramp; from room temperature to 100  $^{\circ}\text{C}$  at 5  $^{\circ}\text{C min}^{-1}$ , followed  
201 by a 30 minute isothermal stage, heated at 2  $^{\circ}\text{C min}^{-1}$  from 100  $^{\circ}\text{C}$  to 520  $^{\circ}\text{C}$ , followed  
202 by a 60 minute isothermal stage and a final ramp at 5  $^{\circ}\text{C min}^{-1}$  to 660  $^{\circ}\text{C}$  followed by a  
203 15 minute isothermal stage. At the time of analysis, 660 $^{\circ}\text{C}$  was the highest possible  
204 temperature achievable by the TG-MS equipment. The consumption rate of gas from  
205 the simultaneous thermo-analyzer can be approximated to 16  $\text{cm}^3\text{min}^{-1}$  helium. The  
206 mass spectrometer was operated in multiple ion detection (MID) mode, monitoring m/z  
207 18 ( $\text{H}_2\text{O}^+$ ), 28 ( $\text{N}_2^+$ ,  $\text{CO}^+$ , including from  $\text{CO}_2$  fragmentation), 32 ( $\text{O}_2^+$ ), and 44 ( $\text{CO}_2^+$ ).  
208 The resulting gas pressure profiles and the temperature profile are shown in Fig. 3(a)  
209 where a baseline corrected background reading has been subtracted from the data. As

210 a result of this data correction, the spectra is used for peak identification rather than a  
211 quantitative analysis. The major constituent of the released volatiles is water, with the  
212 initial release of atmospheric water on the surface of the grains coinciding with the start  
213 of the first temperature ramp and completing during the associated isothermal phase (at  
214 100°C). A second m/z 18 release was observed during the next heating step, with the  
215 peak maximum at 450°C, likely a result of water release from hydrated mineral  
216 impurities. As the temperature was still increasing during this time, 450°C is easily  
217 higher than the temperature required to remove such water from the sample. A small  
218 m/z 44 peak is observed in line with this peak, suggesting decomposition of trace  
219 minerals has been observed. The following suppression of the signal at m/z 44 is then  
220 observed, but this corresponds to a minor artefact in the blank values used to correct  
221 this data and is likely not a true feature. As this is a comparatively limited release of  
222 material over an extended time, these features are relatively small and the m/z 28 peak  
223 that would be expected, corresponding to the m/z 44 peak for CO<sub>2</sub>, is not clearly  
224 observed. The m/z 28 and 32 spectra indicate no clear peaks suggesting they represent  
225 background levels of N<sub>2</sub> and O<sub>2</sub>. As a result of this study, a bake-out temperature of 500  
226 °C was chosen for the following ilmenite experiments. This was expected to remove all  
227 water present from the ilmenite sample before the hydrogen reduction reactions were  
228 performed. This would enable a more accurate quantification of the calculated yield of  
229 oxygen and reduction extent during the ilmenite reduction studies.

230 The bake-out time required was determined by heating a 110.0 mg sample of ilmenite to  
231 500°C at 40°C min<sup>-1</sup> and following this with a 1.5 hour isotherm. The results  
232 (background corrected for blank sample) are shown in Fig. 3 (b). There is a rapid

233 release of volatiles, and therefore higher pressures measured in this experiment  
 234 compared to the previous slower temperature ramp experiment. Using this increased  
 235 heating rate, a sharp m/z 18 peak was observed, with the release appearing completed  
 236 before the isothermal stage, the signal then stabilized as the gases sampled from the  
 237 thermo-analyzer reached equilibrium at the higher temperature. A small peak at m/z 44  
 238 ( $\text{CO}_2^+$ ), and corresponding m/z 28 peak ( $\text{N}_2^+$ ,  $\text{CO}^+$  from fragmentation of  $\text{CO}_2$ ) were  
 239 observed in line with the m/z 18 peak as adsorbed moisture from the air is released. As  
 240 the purpose of this analysis was primarily to identify water release, no specific cleaning  
 241 or drying methods which could potentially affect moisture content were applied to the  
 242 sample before analysis. These analyses do not, therefore, attempt to distinguish if these  
 243 releases are part of the sample or foreign matter. Background levels within the system  
 244 appear to have fully equilibrated by 4000 s, representing approximately 50 minutes into  
 245 the isothermal stage. Total mass loss was approximately 0.35 % of the starting sample  
 246 mass (385  $\mu\text{g}$ ). From this analysis a bake-out time for the ilmenite samples of 1 hour  
 247 was selected.

248



249 **Fig. 3 (a)** The gas release profile for ilmenite when heated up to 660  $^{\circ}\text{C}$  with a variable  
 250

251 *heating ramp. (b) The gas release profile for ilmenite when heated at a rate of 40 °C*  
 252 *min<sup>-1</sup> up to 500 °C followed by a 1-hour isotherm.*

## 253 **2.4 Water calibration**

254 In this work the quantity of water produced from the reduction of ilmenite is estimated by  
 255 measuring the pressure of the water in a sealed system. However, water is susceptible  
 256 to ‘sticking’ to cold spots in the system, where the strong polarity of water molecules  
 257 leads to greater adsorption of water onto surfaces (Pfeiffer Vacuum, 2013). Typically,  
 258 vacuum systems that process water samples are maintained at temperatures of ~100  
 259 °C but to account for the relatively high volumes of water anticipated in the system, the  
 260 manifold was kept at 115 °C to aim to keep water in the vapor phase. However, with the  
 261 need for specific components to operate at cooler temperatures (e.g. valves and  
 262 pressure sensors) it was necessary to characterize the behavior of water vapor in the  
 263 BDM. A calibration study was performed and is detailed in Supplementary Material (S2).  
 264 The results from the study showed that for measured pressures,  $P_m$ , of water < 120  
 265 mbar, the equivalent pressure of water when assuming an ideal gas,  $P_i$ , can be  
 266 calculated as  $P_i = F \times P_m$ . Where  $F$  is a calibration factor defined as follows:

$$267 \quad F = 3.76 \times 10^{-5} \times P_m^2 + 8.79 \times 10^{-4} \times P_m + 1.00 \quad (2)$$

268 At low pressures  $F$  approaches 1, with  $F = 1.03$  at 20 mbar. This calibration  
 269 factor can be applied to determine the pressure that would be observed if water  
 270 produced from ilmenite reduction experiments behaved as an ideal gas and not  
 271 condensing at cold spots. This ideal pressure is used to calculate the yield of oxygen as  
 272 a result of the reactions.

273



## 274 **2.5 Ilmenite reduction experiment parameters**

275 For the following experiments the bake-out temperature of 500 °C and duration of  
276 1 hour had been determined by the TG-MS analysis (section 2.3). A range of ilmenite  
277 masses, 11.2 mg, 23.0 mg, 33.7 mg, and 44.7 mg were reacted, and the quantity of  
278 hydrogen was chosen for all reactions as  $0.30\pm 0.01$  mmol, sufficient to achieve  
279 complete reaction of a 45 mg ilmenite sample (0.3 mmol) according to Eqn. (1). Higher  
280 pressures of hydrogen could increase the extent of water production by maintaining a  
281 water concentration of <10 %, however, the high pressure may also reduce the rate of  
282 diffusion of water away from the reaction site (and thereby smother the reaction). A  
283 manifold temperature of ~115 °C was chosen to aim to keep water in the vapor phase  
284 (see section 2.4). A reaction temperature of 900 °C was chosen as a suitable starting  
285 point for ilmenite reduction studies as it is the minimum temperature required to obtain  
286 reasonable reaction rates (Christiansen et al., 1988) and is within the operating range of  
287 ProSPA. A reaction time of 1 hour was selected as this is within the ProSPA operational  
288 power and time requirements.

289

## 290 **2.6 Ilmenite reduction experimental procedure**

291 To determine if ilmenite can produce water in a static system, different quantities  
292 of ilmenite were heated in the presence of hydrogen. Any water produced as a result of  
293 this reaction, was condensed at the cold finger (see Fig 1b). After the duration of the  
294 experiment the cold finger was then heated to release the water which was measured  
295 via a pressure sensor. Ilmenite is reacted in these studies to quantify the water that can  
296 be produced from the reduction of the iron oxide bearing mineral. Although the ilmenite

297 used in this work contains 5% other mineral traces, the effects on the reaction of such  
298 impurities are assumed to be minimal. The interfering factors arising from the inclusion  
299 of other lunar minerals will be investigated in future work with lunar simulants and  
300 samples. The steps for each ilmenite reduction reaction were:

301 **Sample Loading:** The weighed sample was loaded into the ceramic oven and  
302 attached to the BDM and evacuated to a pressure  $<10^{-6}$  mbar as  
303 measured at the vacuum pump.

304 **Bake-out:** The oven was heated to a bake-out temperature of 500 °C for 1 hour  
305 to remove any volatiles and the pressure of released volatiles was  
306 measured. After the bake-out, the volatiles were evacuated through  
307 vacuum pumps via valve 8.

308 **Hydrogen Addition:** ~ 0.3 mmol of hydrogen gas was introduced into the BDM

309 **Reaction:** The cold finger was cooled to -180 °C and the oven was heated to  
310 the reaction temperature of 900 °C. During the 1 hour reaction the  
311 residual pressure of hydrogen was measured continuously by  
312 monitoring the gauge p1.

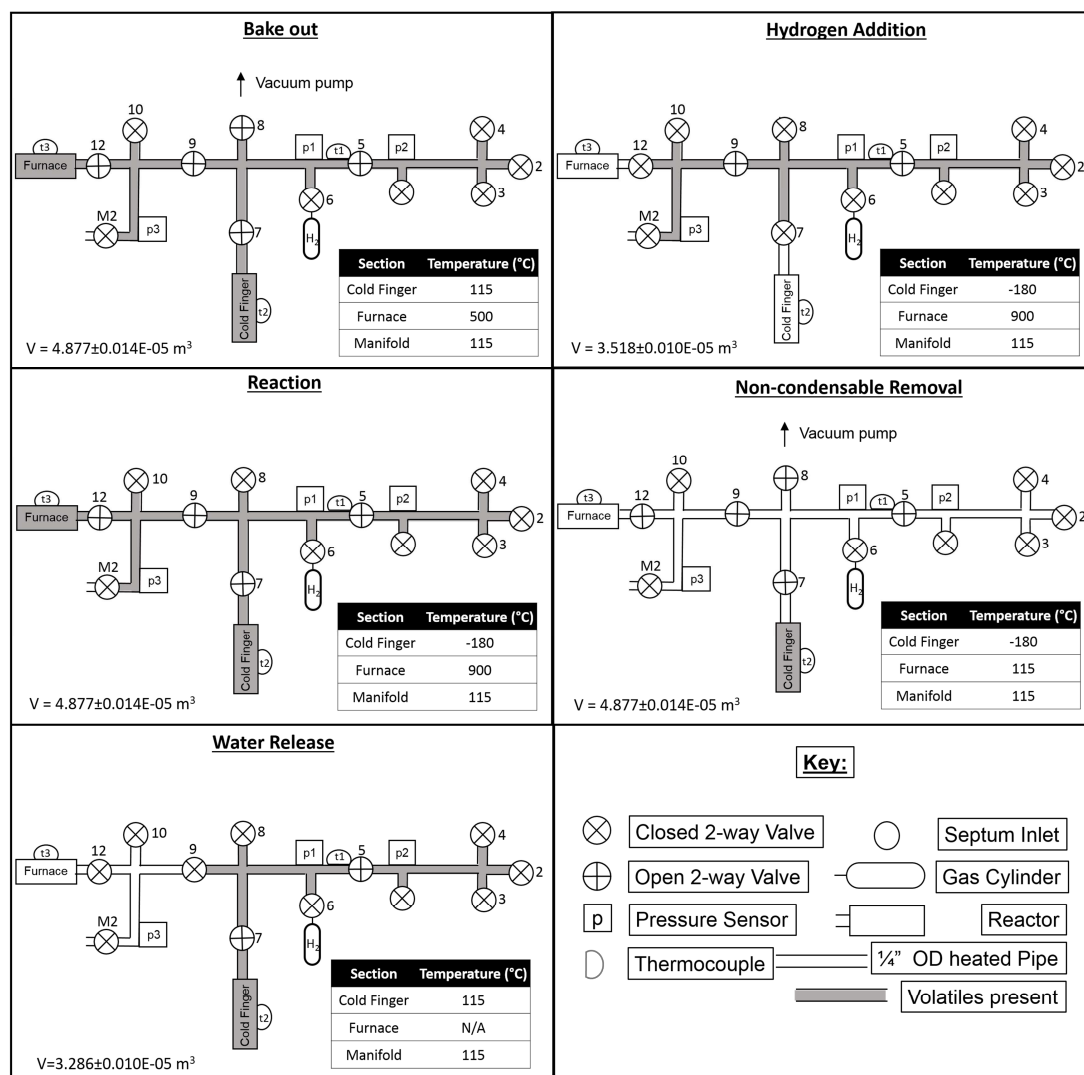
313 **Non-Condensable Removal:** The hydrogen (and any non-condensable volatiles)  
314 were removed by pumping to vacuum, as measured at the vacuum  
315 pump.

316 **Water Release:** The cold finger was heated to 115 °C at a rate of  $\sim 125$  °C  $\text{min}^{-1}$  and  
317 the amount of water produced measured on gauge p1.

318 Post reaction: Once the oven had cooled to room temperature, grains were  
319 removed from the oven and prepared for Scanning Electron  
320 Microscope (SEM) analysis.

321 An outline of the experimental procedure is shown in Fig. 4. It should be noted that the  
322 assumed average system temperature used for analysis is taken to be 115 °C. Although  
323 valves and pressure sensors may be operating at lower temperatures, they represent  
324 relatively small volumes of the entire system.

325



326  
 327 *Fig. 4 Volumes and temperatures for each phase of the ilmenite reduction study, where*  
 328 *the cold finger, furnace, and manifold are separately thermally controlled.*

329  
 330 After each experiment, ilmenite grains were analyzed for evidence of the  
 331 reduction reaction. A random selection of grains from each reacted sample, and an  
 332 unreacted sample were set in epoxy resin in 10 mm brass rings and then polished and  
 333 carbon-coated for analysis using a FEI Quanta 200 3D FIB-SEM.

### 334 **3 Gas Transport Analysis**

335 To determine the extent to which ilmenite reduction reactions are feasible with  
 336 ProSPA, two models were used to identify the time scales involved for the produced  
 337 water to diffuse through the system. The gas flow type and consequently the diffusion  
 338 rate are discussed. The flow of molecules in a vacuum system can be characterized as  
 339 either viscous, transitional, or molecular flow. Once the type of flow has been  
 340 established, it is possible to estimate the time taken for the water molecules produced in  
 341 the reaction to be replaced by hydrogen molecules, and for the reaction to continue.  
 342 The Knudsen number,  $K_n$ , is used to characterize the flow of gas within a system as  
 343 follows (Delchar, 1993):

$$\begin{aligned} \text{Viscous flow} & \quad K_n < 0.01 \\ \text{Transitional flow} & \quad 0.01 \leq K_n \leq 1 \\ \text{Molecular flow} & \quad K_n > 1 \end{aligned}$$

344 The Knudsen number for the flow of water from the furnace to the cold finger in the  
 345 ProSPA system was estimated for a simplified pipe of length  $l$ , radius  $r$ , and uniform  
 346 temperature,  $T$ , where the volume of the pipe,  $V$ , is defined as  $V=l\pi r^2$ .

347 Eqn. (3) is used to calculate the Knudsen number for a system where  $\lambda$  is the mean free  
 348 path of a gas particle and  $a$  is the radius of the pipe.

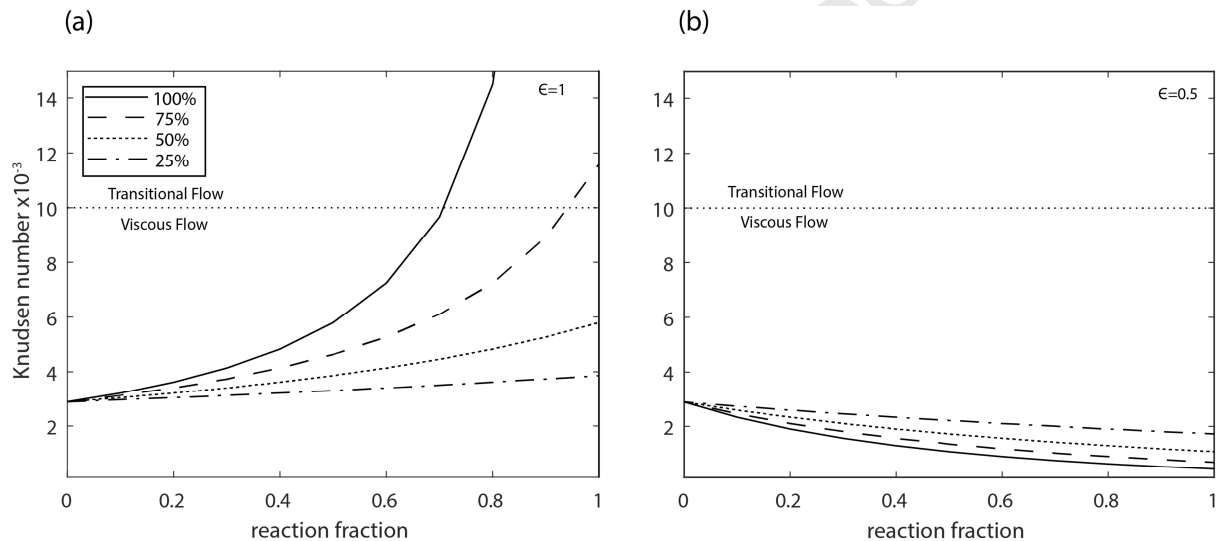
$$349 \quad K_n = \frac{\lambda}{a} \quad (3)$$

350 The calculations and data used to determine the mean free path of gas molecules  
 351 expected in the system is outlined in more detail in Supplementary Material (S3). A  
 352 trapping efficiency  $\epsilon$  is considered which determines how much of the produced water is

353 condensed at the cold finger, where a value of 1 means 100% of the water is  
 354 condensed.

355

356 The Knudsen number was determined for the ilmenite concentrations trialled in  
 357 this work, 25%, 50%, 75% and 100% of the 45 mg standard mass. A pipe of length 1 m  
 358 and internal diameter of 4 mm is assumed. As the trapping efficiency is unknown, a  
 359 trapping efficiency of 0.5 and 1 are shown in Fig. 5.



360

361 *Fig. 5 Knudsen number for a range of ilmenite concentrations throughout the reduction*  
 362 *reaction considering a trapping efficiency of (a)  $\epsilon = 1$ , and (b)  $\epsilon = 0.5$ .*

363 When it is assumed that all the water produced is immediately condensed ( $\epsilon=1$ ), the  
 364 Knudsen number increases as a result of the lower pressure in the system. However,  
 365 when only 50 % of the water produced is condensed ( $\epsilon=0.5$ ), the relative proportions of  
 366 water molecules to hydrogen molecules increases, which leads to an increase in the  
 367 average diameter of molecules in the system with time and the gas flow becomes more  
 368 viscous. It is assumed that the gas flow will be mostly viscous and so water must first

369 diffuse through the hydrogen gas before collecting at the cold finger. To estimate the  
 370 diffusion rate of water from the reactor to the cold finger, a simple model was  
 371 considered with a partial pressure of 10 % water vapor at the furnace and 0% water  
 372 vapor at the cold finger. A partial pressure of 10 % was chosen as a boundary condition  
 373 in line with the assumptions contained within Taylor et al., 1993).

374 The diffusion rate can be derived from the molar flux of water (gas A) into hydrogen  
 375 (gas B) using Eqn. (4), which is adapted from Fick's law in Geankoplis (1993).

$$376 \quad J_{AZ} = D_{AB} \frac{(P_{A1} - P_{A2})}{RT(z_2 - z_1)} \quad (4)$$

377  $J_{AZ}$  is the molar flux of gas A,  $D_{AB}$  is the diffusion coefficient which defines the molecular  
 378 diffusivity of gas A in gas B,  $R$  is the molar gas constant,  $T$  is the average temperature  
 379 of the system (K), and  $z_2 - z_1$  is the distance of diffusion.  $P_{A1}$  and  $P_{A2}$  are the pressures  
 380 of gas A within the furnace volume and at the cold finger respectively, assuming  $P_{A2}$  is 0  
 381 Pa for a first order approximation.  $P_{A1}$  is derived from the ideal gas law using the pipe  
 382 volume,  $V$ , the pipe temperature,  $T$ , and the total number of moles of water produced  
 383 presumed to be at the start of the pipe,  $n_A$ .  $n_A$  is defined as 10% of the moles of  
 384 hydrogen in the system,  $n_B$ .

385 The molar flux of water into hydrogen can be used to determine the time of  
 386 diffusion,  $t$ , across the length of the pipe using the concentration of water molecules in  
 387 the pipe,  $C_A$  as in Eqn. (5):

$$388 \quad t = \frac{l \cdot C_A}{J_{AZ}} \quad (5)$$

389 The calculations and data used to determine the diffusion time in the system are  
 390 outlined in more detail in S4.

391 With 0.3 mmol of H<sub>2</sub> (translating to a system pressure of ~198 mbar) and a partial  
 392 pressure limit of 10% of water at the furnace, the calculated diffusion time is ~170 s (1.8  
 393 μmol s<sup>-1</sup>. Providing the diffusion of water vapor away from the reaction site is the rate  
 394 controlling step, this suggests that all the water that can be produced from the reduction  
 395 of 45 mg of ilmenite can be collected on the time scale of a few hours and therefore be  
 396 feasible within the ProSPA system. There are limitations to these models but they  
 397 provide a good first order analysis of the feasibility of the reaction.

398

### 399 **3 4Results**

400 The reaction and water release phases of each individual ilmenite reduction  
 401 experiment are considered below in detail.

#### 402 **4.1 Ilmenite reduction: Reaction Phase**

403 Following bake-out, the ilmenite is reacted for 1 hour with 0.3 mmol of hydrogen  
 404 at 900 °C. The pressure profiles during the reaction of each sample is shown in Fig. 6.  
 405 The hydrogen present in the system should react with the ilmenite to produce water in  
 406 an equal number of moles (1), which in itself should result in no net change in the  
 407 pressure of the system. However, with the cold finger operating at -180 °C, this water is  
 408 condensed at the cold finger removing water from the gaseous phase and reducing the  
 409 pressure in the system. Therefore, a pressure drop is recorded, corresponding to the  
 410 conversion of H<sub>2</sub> to H<sub>2</sub>O and the subsequent removal of gaseous H<sub>2</sub>O by the cold trap.  
 411 An estimated quantity of H<sub>2</sub> in moles,  $n_h$ , that has reacted is also shown in Fig. 6,  
 412 calculated from the ideal gas equation where:

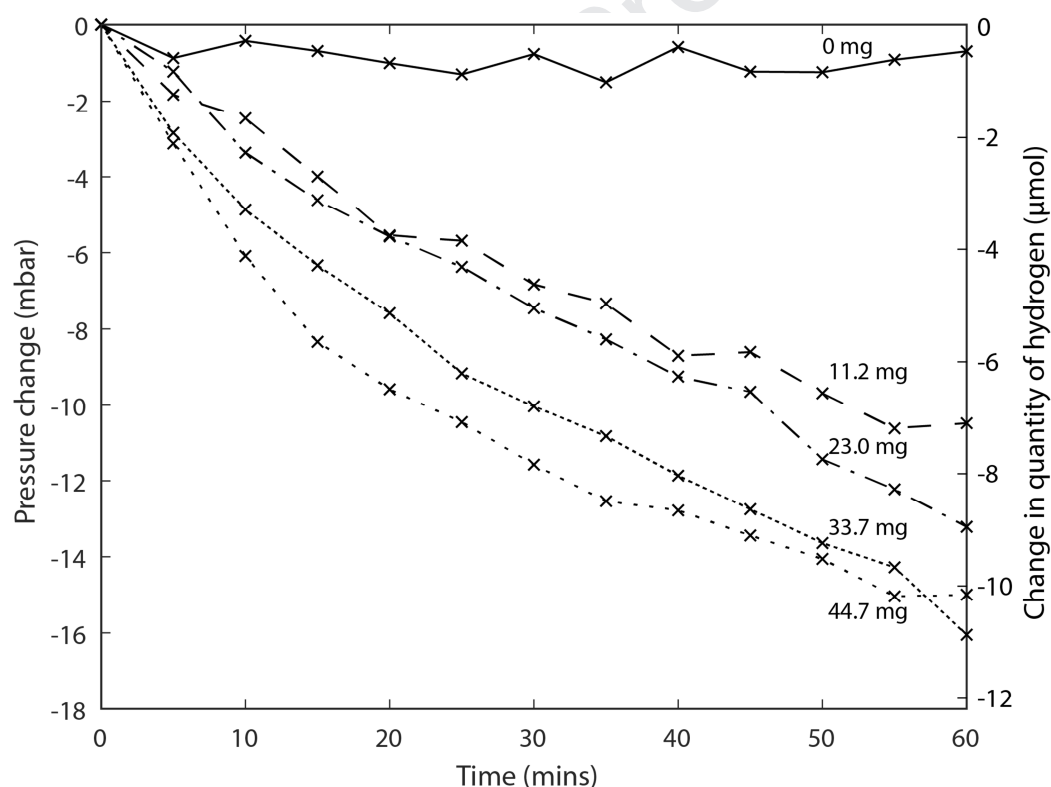
$$413 \quad n_{h|w} = \frac{p \times V}{R \times T} \quad (6)$$



414 Where  $p$  is the pressure in the system with an uncertainty of  $\pm 1$  mbar, the volume of the  
 415 system  $V$  is taken from Fig. 4,  $R$  is the ideal gas constant, and the assumed  
 416 temperature of the system  $T$  is at  $115\text{ }^\circ\text{C}$  ( $388\text{ K}$ ).

417 The initial and final pressure in the system is recorded in Table 1 for each sample, along  
 418 with the calculated amount of hydrogen that has reacted. It can be assumed that during  
 419 the reaction the gases were moving in the viscous flow regime as pressures of  $> 105$   
 420 mbar were recorded (Pfeiffer Vacuum, 2013).

421 The results show that with increasing ilmenite mass the pressure change increases,  
 422 showing that more hydrogen has been converted to water. The pressure is still dropping  
 423 after 60 minutes indicating the reaction has not neared completion in this time.



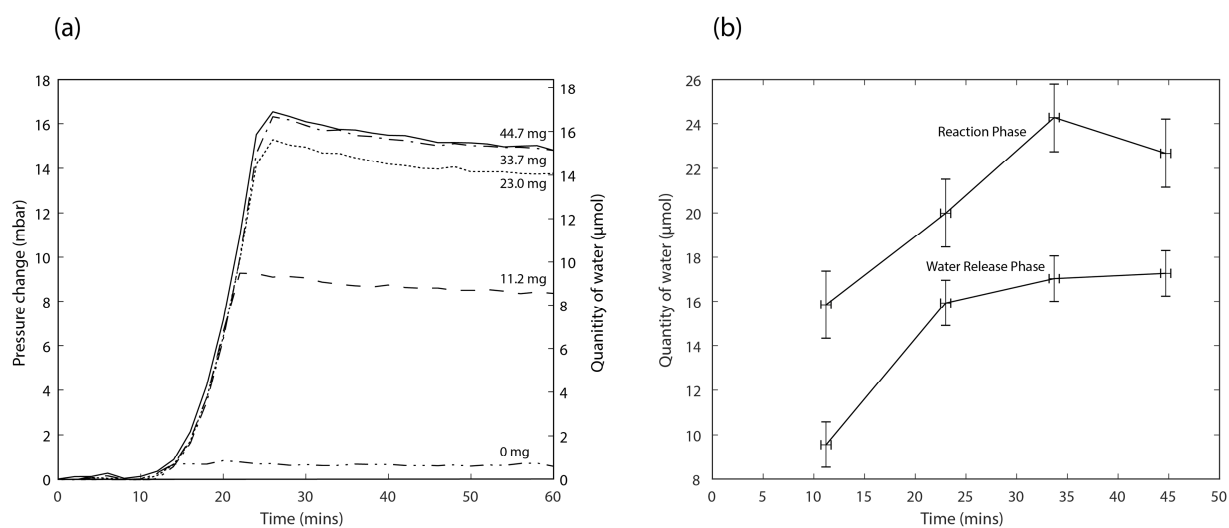
424  
 425 Fig. 6 Pressure change and equivalent change in amount of hydrogen with time during  
 426 the reaction phase with varying masses of ilmenite.

## 427 **4.2 Ilmenite reduction: Water release phase**

428           The final phase of the experiment, the water release stage, is where the cold  
429 finger is heated to 115 °C and the pressure in the system is recorded for 1 hour. As the  
430 cold finger is heated quickly ( $\sim 125 \text{ }^\circ\text{C min}^{-1}$ ) from -180 °C to 115 °C, there is a small  
431 peak at  $\sim 5$  minutes where water is likely released and re-condensed on a cold spot as a  
432 result of non-uniform heating of the cold finger. It takes a further  $\sim 10$  minutes for the  
433 pressure in the system to start to rapidly increase as condensed volatiles are re-  
434 released as gases into the system (Fig. 7a). The initial pressure rise is then followed by  
435 a downward drift in pressure. With increasing ilmenite mass, the peak pressure  
436 increases because of more volatiles being released. For higher ilmenite masses, the  
437 pressure profiles are limited to  $\sim 16$  mbar. It is assumed that the pressure rise during the  
438 water release stage is wholly as a result of water vapor produced from the ilmenite  
439 reduction reaction. The equivalent production of water  $n_w$  from each ilmenite sample is  
440 calculated using Eqn. (6), by assuming the associated pressure rise is a result of the  
441 production of water only, and included in Fig. 7(a). The amount of hydrogen reacted to  
442 produce water from the reaction phase is compared to the amount of water produced  
443 from the water release phase and shown in Fig. 7(b). Uncertainties are calculated using  
444 the propagation of uncertainties from the manifold temperature ( $\pm 5^\circ\text{C}$ ), volume (Fig. 4),  
445 and pressure values ( $\pm 1$  mbar). The temperature uncertainty is derived from the  
446 variation in manifold temperature, the volume uncertainty is derived from the standard  
447 deviation in volume calculations performed from the expansion of gases in the system,  
448 and the pressure uncertainty is derived from the uncertainty of the sensor. The reaction  
449 phase data suggests that more hydrogen is reacted (and therefore water produced)

450 than compared to the water release data. One cause for this discrepancy would be  
451 inefficient trapping of water at the cold finger, perhaps water sticking in the system  
452 before reaching the cold finger. All pressure and equivalent water quantity data are  
453 shown in Table 1, along with a calibrated pressure value as determined using Eqn. (2).

454



455

456 Fig, 7(a) Pressure rise and equivalent water production with time during the water  
457 release phase with varying masses of ilmenite. (b) Estimated water produced from  
458 varying ilmenite masses as calculated from pressure data during the reaction and water  
459 release phases with a  $1\sigma$  uncertainty.

### 460 4.3 Calculation of the reaction yield and efficiency

461 Although water is the product of the reduction reaction, its constituent oxygen is  
462 the resource most commonly referenced when discussing yields. There are many ways  
463 in which “yield” can be calculated. For instance, yield could be the mass of oxygen  
464 extracted compared to the sample mass, or the mass of oxygen extracted compared to  
465 the total oxygen in the sample, or the mass of oxygen extracted compared to the

466 maximum amount of oxygen that can be extracted (Eqn. 1). In addition, the yield can  
467 be calculated as the mass of water extracted.

468 Here “yield” is defined as the wt. % of oxygen extracted compared to the total sample  
469 mass, from here described as calculated oxygen yield (7). This term is more useful for  
470 ISRU and a mining perspective as the desired product is commonly oxygen and in this  
471 case it indicates the total mass of ilmenite that needs to be present in the regolith to  
472 obtain a certain quantity of oxygen. The calculated oxygen yield is the ratio between the  
473 mass of oxygen produced,  $m_o$ , with respect to the mass of ilmenite started with,  $m_{ilm}$ ,  
474 The mass of oxygen produced can be calculated from the mass of water produced,  $m_w$ ,  
475 by multiplying it by the ratio between the molar mass of oxygen,  $M_o$ , and the molar mass  
476 of water,  $M_w$ . The amount of water produced,  $n_w$ , can be substituted for  $m_w/M_w$  and can  
477 be calculated with Eqn. 7 and the pressure rise from the water release phase. In theory  
478 the maximum yield of oxygen from water for the ilmenite reduction process as given in  
479 Eqn. (1) is 10.5 wt. % oxygen.

$$480 \text{ yield} = \frac{m_o}{m_{ilm}} = \frac{m_w M_o}{m_{ilm} M_w} = \frac{n_w M_o}{m_{ilm}} \quad (7)$$

481 When comparing the efficiency of a particular reaction it is more useful to measure the  
482 extent of the reduction reaction,  $\xi$ , derived from the ratio of the mass of oxygen  
483 produced,  $m_o$ , with respect to the maximum potential oxygen produced,  $m_{o,max}$ . The  
484 reduction extent is therefore equivalent to the amount of water produced as a  
485 percentage of the total water that could be produced by the reaction (Eqn. 8).

486

$$487 \xi = \frac{m_o}{m_{o,max}} = \frac{m_o M_{ilm}}{M_o m_{ilm}} \quad (8)$$

488 The yield outputs are summarized in Table 1 and Fig. 8, where the uncertainties are  
 489 derived as in Fig. 7b. Maximum yield and reduction extent occurs in smaller masses of  
 490 ilmenite. For a mass of 11.2 mg, peak oxygen yields of  $2.3 \pm 0.2$  wt. % and  $1.4 \pm 0.2$  wt. %  
 491 are calculated for the reaction phase and water release phase respectively, equating to  
 492 reduction extents of  $21.5 \pm 2.3$  % and  $12.9 \pm 1.5$  % respectively.

493

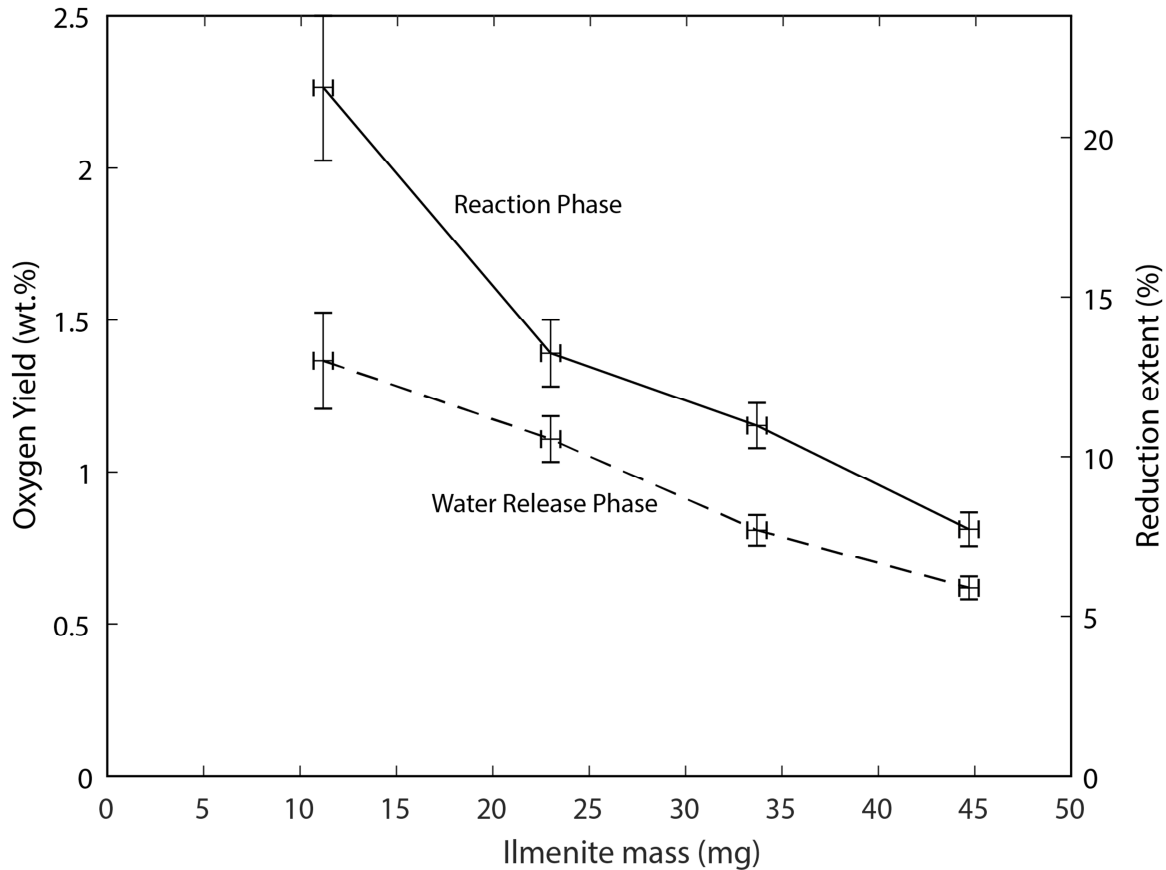
			Ilmenite mass (mg)				
			0	11.2± 0.5	23.0± 0.5	33.7±0.5	44.7±0.5
<b>Reaction phase</b>	Hydrogen pressure (mbar)	Initial	170.3± 1.0	171.0± 1.0	163.7± 1.0	168.9± 1.0	167.3± 1.0
		Final	169.6± 1.0	160.5± 1.0	150.5± 1.0	152.8± 1.0	152.3± 1.0
		Difference	0.7± 1.0	10.5± 1.0	13.2± 1.0	16.0± 1.0	15.0± 1.0
	Calculated hydrogen reacted (μmol)		1.0± 1.5	15.8± 1.5	20.0± 1.5	24.3± 1.5	22.7± 1.5
	Oxygen yield (wt. %)		n/a	2.3±0.2	1.4±0.1	1.2±0.1	0.8±0.1
	Reduction extent (%)		n/a	21.5±2.3	13.2±1.0	10.9±0.7	7.7±0.5
<b>Water release phase</b>	Pressure rise (mbar)	Measured	0.8± 1.0	9.3± 1.0	15.3± 1.0	16.3± 1.0	16.5± 1.0
		Calibrated	0.8± 1.0	9.4± 1.0	15.5± 1.0	16.6± 1.0	16.8± 1.0
	Calculated water produced (μmol)		0.8±1.0	9.5±1.0	15.8±1.0	16.9±1.0	17.1±1.0
	Oxygen yield (wt. %)		n/a	1.4±0.1	1.1±0.1	0.8±0.1	0.6±0.1
	Reduction extent (%)		n/a	12.9±1.5	10.4±0.7	7.6±0.5	5.8±0.4

494 *Table 1. Details of the results for each ilmenite sample during the reaction phase and*  
 495 *water release phase. Included are the pressure changes recorded, the calculated*

496 amount of hydrogen used in the reaction, and the calculated amount of water produced.

497 Oxygen yield and reduction extent are also included.

498



499

500 *Fig. 8 Calculated yield and reduction extent derived from the reaction phase and from*  
501 *the water release phase with a 1 $\sigma$  uncertainty.*

502

#### Section 4.4 Ilmenite grain analysis

503

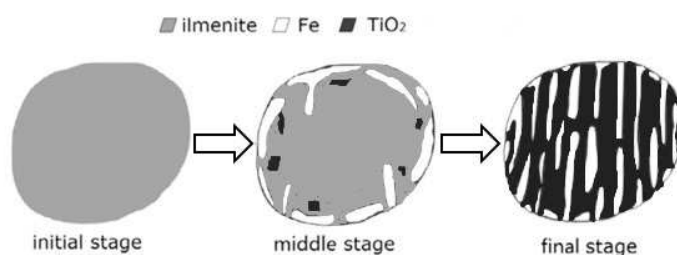
504

505

506

The process of ilmenite reduction can be described by a shrinking core model as shown in Fig. 9 by Dang et al. (2015). The reaction of ilmenite proceeds from the surface to the interior of the grain as hydrogen diffuses inwards, reduces the ilmenite, and water diffuses out of the grain. Metallic iron forms on the outer edges of the grains

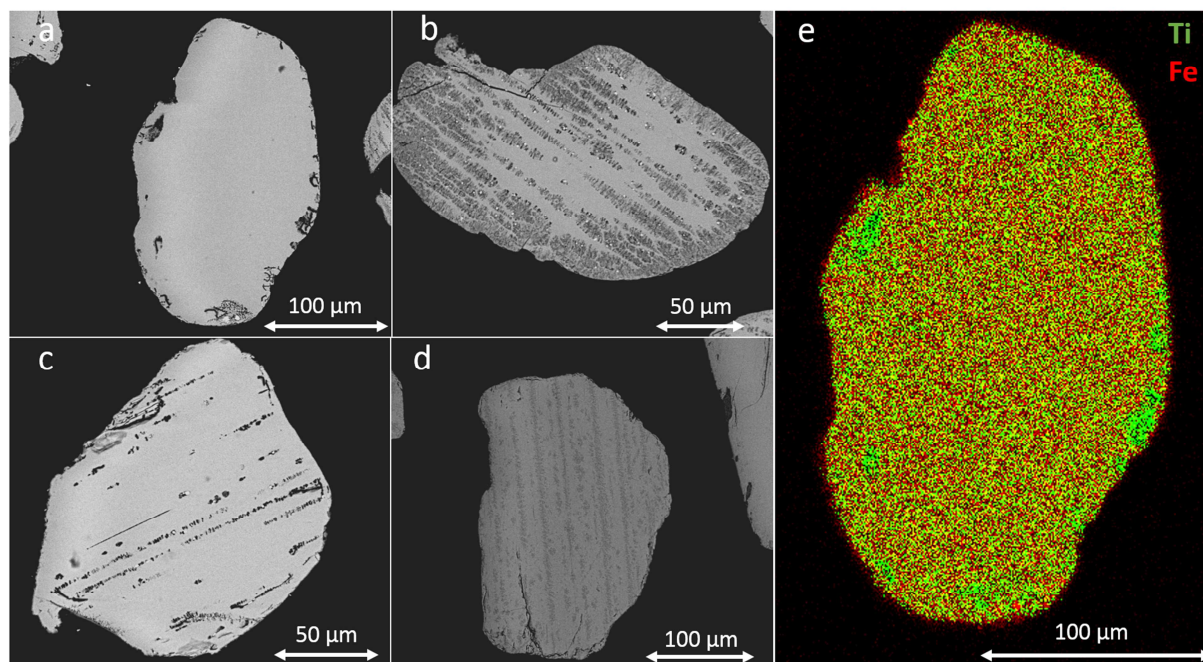
507 where the reaction has occurred, acting as a nuclei for further metallic iron formation  
 508 towards the center of the grains. The shrinking core model suggests that reduction  
 509 would occur quickly at first, as a larger surface area of ilmenite is exposed to hydrogen.  
 510 As the reaction progresses the reduction process slows as the surface area decreases;  
 511 in addition, hydrogen gas must diffuse through the reacted layer to access unreacted  
 512 ilmenite and water needs to diffuse through the reacted layer to be removed. Zhao &  
 513 Shadman (1993) discuss three stages of the reduction process; namely induction,  
 514 acceleration and deceleration. The induction stage, a result of initially slow transport of  
 515 iron from the ilmenite pores, is followed by an accelerated reaction rate until the ilmenite  
 516 supply decreases to a point where the reaction is decelerated.



517  
 518 *Fig. 9 Ilmenite grain reduction by hydrogen via the shrinking core model, adapted from*  
 519 *Dang et al. (2015).*

520 Approximately 15 mg of unreacted ilmenite grains were studied by Back Scatter  
 521 Electron (BSE) imaging using a SEM (Fig. 10 a-d) where the contrast in gray-scale  
 522 highlights differences in the average atomic numbers of constituent elements (Goldstein  
 523 et al. 2017). Heavy elements such as Fe appear brighter as a result of a stronger  
 524 backscatter of electrons. Some grains appear to have non-uniform chemical  
 525 composition. They display lamellar features (likely rutile) corresponding to darker BSE

526 regions. An X-ray multi-element map of an unreacted grain (Fig. 10 e) shows relatively  
527 homogeneous distribution of Fe and Ti contents with some Ti hotspots.

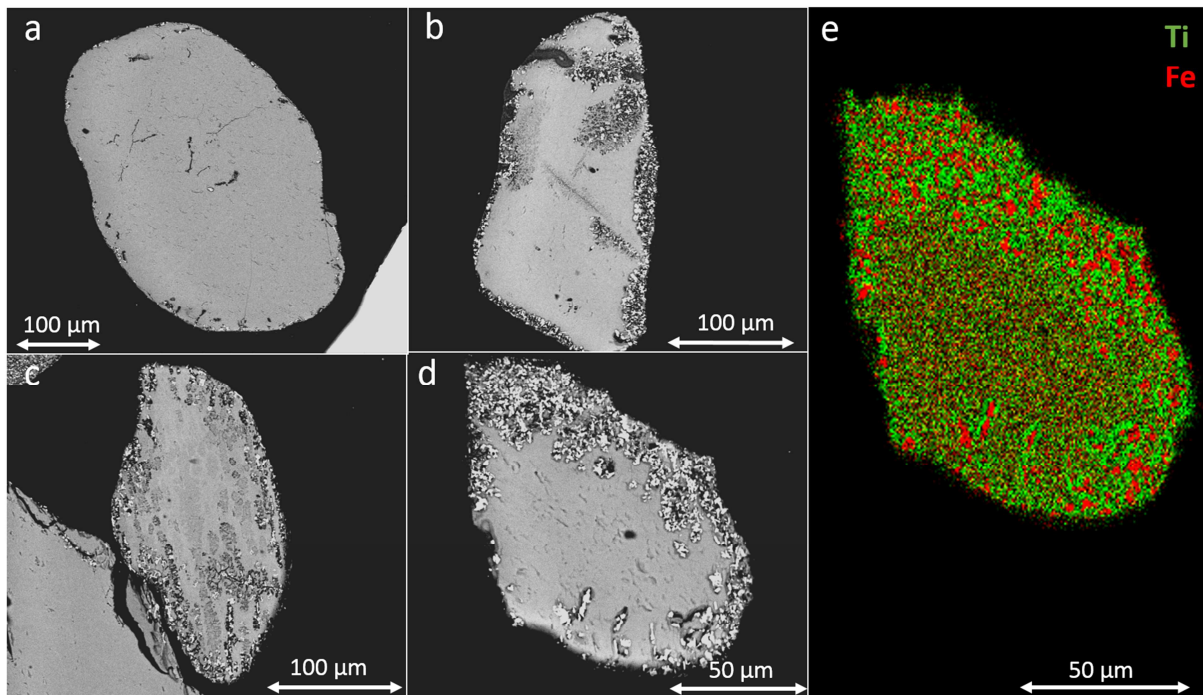


528  
529 *Fig. 10 (a-d) Example BSE images of unreacted ilmenite grains. (e) Ti and Fe element*  
530 *map of grain a.*

531 The reacted ilmenite samples were also analyzed using BSE. Approximately 15  
532 mg was used for analysis from each sample, where the grains represent a random  
533 selection from across the sample, and where the placement of the grains in the reaction  
534 tube is not known. The reaction proceeded different amounts in different grains, likely a  
535 result of their location within the tube. The reacted grains show further darkening in  
536 terms of their BSE response and the production of bright spots (Fig. 11 a-d). There is  
537 also a darkening and formation of bright spots on the edge of the grains. The darker  
538 areas have a higher proportion of titanium whilst the brighter spots show an increase in  
539 iron. It is likely that the lamellae can provide a pathway for hydrogen into the ilmenite



540 structure as they are a physically separate mineral structure within the main mineral  
541 structure. A reaction front can be seen moving inwards from the surface and producing  
542 metallic iron. This suggests that the reduction reaction occurs preferentially from the  
543 outside in, as shown by Dang et al. (2015), and along the lamellae supporting the  
544 shrinking core model (Fig. 9). An element map of one of the reacted grains (Fig. 11 e)  
545 show areas of concentrated Ti and depleted Fe, suggesting that Fe has been separated  
546 from the ilmenite leaving a  $\text{TiO}_2$  residue. This trend follows the grain from the outside in,  
547 representing the extent to which the reaction has penetrated into the grain.



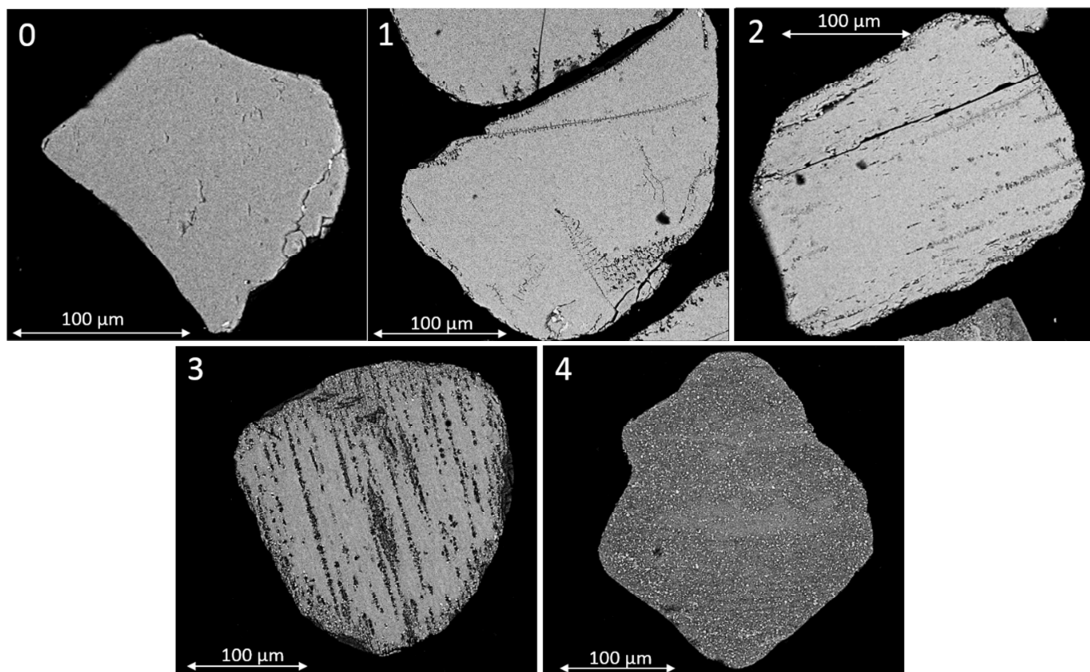
548

549 *Fig. 11 (a-d) Example BSE images of reacted ilmenite grains taken from the 23.0 mg*  
550 *ilmenite sample. (e) Ti and Fe element map of grain d.*

551 Each reacted sample was imaged using BSE. At a 500x zoom, two images were  
552 taken of random groups of grains for each reacted sample. The reduction extent was

553 determined using a scale from 0-4 (Fig. 12). The fraction of grains assigned to each  
554 classification was then compared for each sample (Fig. 13). The fraction of grains for  
555 each sample represent ~7%, 3%, 3%, and 2% of the 11.2 mg, 23.0 mg, 33.7 mg, and  
556 44.7 mg sample respectively. As the grains imaged are from a random selection from  
557 each sample, it is assumed that each analyzed image is representative of the entire  
558 bulk sample.

559

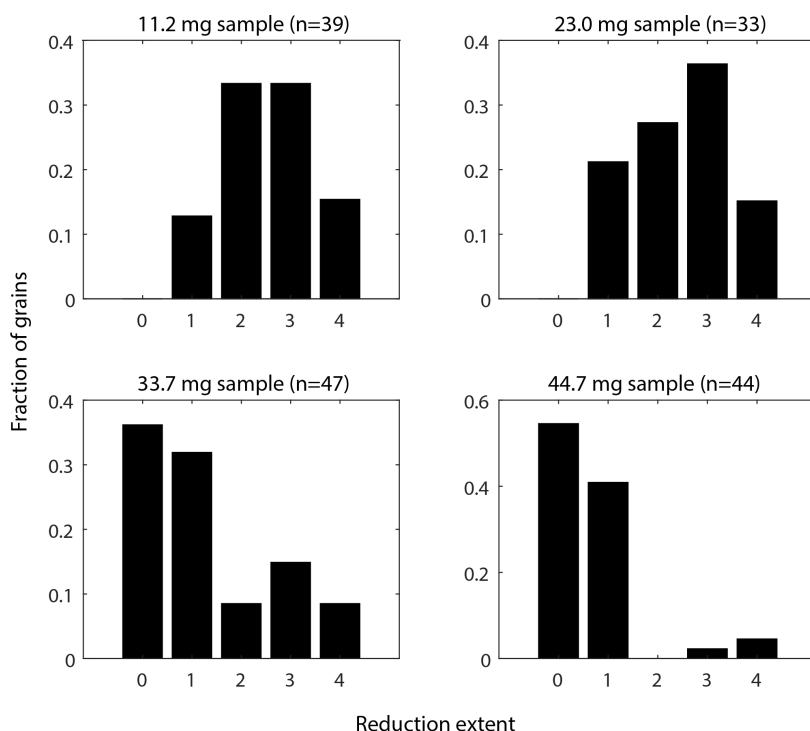


560

561 *Fig. 12 Reduction extent scale where 0 shows no reaction, 1 shows partial reaction of*  
562 *the outer rim of the grain, 2 shows full reaction on the outer rim of the grain, 3 shows*  
563 *significant penetration of reaction into the grain, and 4 shows complete reaction of the*  
564 *grain.*

565

566



567

568 *Fig. 13 Histograms displaying the distribution of reduction extent, as defined by the*  
 569 *extent of the reduction reaction around and into the grain, as a fraction of the number of*  
 570 *grains for each sample size*

571 **5 Discussion**

572 The bake-out process was demonstrated to successfully remove volatiles from  
 573 ilmenite samples (See Supplementary material S.5). As a result, any volatiles measured  
 574 during the reaction and water release phases are likely only associated with the ilmenite  
 575 reduction process. It is therefore recommended that when ilmenite reduction is  
 576 performed on the lunar surface within ProSPA, a bake-out process be incorporated into  
 577 the extraction of trapped water ice and/or solar wind implanted particles (SWIP) from  
 578 the lunar regolith, and the volatiles would be analyzed and stored.

579 The reaction stage showed a greater hydrogen pressure drop in the system for larger  
580 samples (15.0 mbar pressure drop for 44.7 mg ilmenite) compared to the smaller  
581 samples (10.5 mbar pressure drop for 11.2 mg ilmenite) suggesting that more ilmenite  
582 has reduced to produce water which is then condensed. There is only one data set per  
583 sample mass available, however they appear to follow a predictable trend. As the  
584 pressure continues to drop for the entire 1 hour reaction time, it is assumed that the  
585 reaction has not reached completion. As the amount of H<sub>2</sub> present in each study (0.3  
586 mmol) is stoichiometrically sufficient to reduce a 45 mg (0.3 mmol) ilmenite sample, the  
587 smaller ilmenite samples will have an excess of hydrogen. The quantity of hydrogen  
588 was kept consistent so that the reaction pressures were consistent between  
589 experiments. It is assumed that only when the reactions are near completion will having  
590 an excess of hydrogen be relevant to the reaction rates. This would be confirmed with  
591 longer experiments. With the current setup and assuming as a first order analysis that  
592 the reaction rate is linear, it would take over 12 hours for the 45 mg ilmenite sample to  
593 completely reduce. This is not suitable for the ProSPA instrument and adaptations to  
594 the experiment will be required.

595 The water release phase showed the pressure peaks are limited to ~16 mbar which  
596 is well within the linear pressure range (~80 mbar) as identified in the water calibration  
597 tests. When the calibration factor,  $F$ , was applied there was  $\leq 0.3$  mbar increase in the  
598 pressure value. This suggests that almost all the water released from the cold finger is  
599 being detected by the pressure sensor, and not condensing elsewhere in the system.

600 The series of experiments showed that the water yield to ilmenite mass ratio is not  
601 1:1. The smaller samples produce more water per unit mass of ilmenite compared to the

602 larger samples. For example, a sample of 11.2 mg (25% of 44.7 mg) produced 55% of  
603 the amount of water produced by the 44.7 mg sample. It is possible that the smaller  
604 samples are not as compacted at the bottom of the ceramic tube as the larger samples,  
605 enabling greater movement of gases to and from the reaction sites. Both the reaction  
606 phase and water release phase data sets show that at  $> \sim 30$  mg of sample the reaction  
607 does not appear to produce significantly more water. This suggests that within a static  
608 system hydrogen cannot penetrate below a certain depth. In this case, a 30 mg sample  
609 equates to a depth of ilmenite sample of  $\sim 2.3$  mm with a defined grain size of  $\sim 170$   $\mu\text{m}$ .  
610 It is assumed that produced water cannot diffuse away quickly enough from below this  
611 depth and the reaction is suppressed. A delayed pressure rise in the system (Fig. 7a)  
612 during the water release phase suggests that water is initially released and re-  
613 condensed at a cold spot higher in the cold finger, which is as a result of thermal lag.  
614 Once the cold finger is uniformly heated, a significant release of volatiles is measured.

615 As seen in Fig. 8, a constant decrease in oxygen yield (as a wt. % of the original  
616 sample) with ilmenite mass shows that the smaller samples are closer to reaction  
617 completion than the larger samples. As no sample produced the maximum possible of  
618 10.5 wt.% oxygen, it supports the idea that the reaction does not complete in 1 hour  
619 with the defined system characteristics. A higher reaction temperature and potentially  
620 longer reaction times should lead to higher yields when operating at these low  
621 pressures as more ilmenite is reduced.

622 The yield calculated from the drop in hydrogen pressure during the reaction is greater  
623 than the yield calculated from the vapor release from the cold finger. This suggests that  
624 not all the water produced during the reaction is condensed at the cold finger. One

625 major difference in the operational volume between the reaction phase and the water  
626 release phase, is that the furnace is only included in the reaction phase. Therefore, if  
627 water is trapping on cooler pipework between the hot furnace and the valve connecting  
628 it to the rest of the system, then this water would not be included in the yields measured  
629 in the water release phase. The trapping and releasing of water is on average ~68 %  
630 efficient when comparing the difference in pressure changes recorded in each phase. It  
631 is suggested that a future version of the BDM be built with increased thermal control to  
632 minimize such condensation of water in undesirable locations.

633 BSE images were used to identify metallic iron formation as an indicator of where the  
634 reaction has occurred. As the reacted grains do not show the presence of metallic iron  
635 in all areas, the reaction is likely incomplete, which was suggested from the pressure  
636 readings and yield calculations. The grains do not appear to have reacted uniformly in  
637 each ilmenite sample. Looking at a random selection of grains from each experiment  
638 shows that smaller samples reacted more completely than larger samples. Some grains  
639 appeared mostly unreacted, while others were extensively reacted, supporting the  
640 suggestion that reactants and products cannot move easily below a certain depth of  
641 ilmenite grains. It is not practical to select grains from the top or bottom of the sample  
642 holder specifically for this to be confirmed, as a result of the narrow dimensions of the  
643 sample holder. If the average ilmenite grain size were smaller, which could be the case  
644 on the lunar surface (McKay et al., 1991), the reaction rate would likely increase as the  
645 surface area increases, and the distance of gas diffusion required through the interior of  
646 the grains is reduced, although smaller grain sizes would also result in a longer diffusion  
647 pathway between grains. A wider sample holder, and/or smaller grain size could

648 potentially enable greater penetration of hydrogen gas into the sample, and quicker  
 649 removal of water from the reaction site, potentially increasing the sample size limit of the  
 650 reaction and increasing the reaction rate.

651 The reaction efficiency of the BDM is relatively low, producing up to 1.4 wt. % oxygen  
 652 from relatively pure ilmenite. Meanwhile, other ISRU technologies such as PILOT and  
 653 ROxygen could produce similar yields from regolith (Sanders and Larson, 2012).  
 654 However, the reaction procedure used in this work was not optimized for greatest yields.  
 655 The system successfully reduced iron bearing minerals to produce and collect water.  
 656 The next steps will require optimization of the system and procedure so it is capable of  
 657 reducing samples with lunar-like composition.

658 A lunar surface sample will likely contain  $\leq 20$  % by volume ilmenite, where a highland  
 659 sample would likely have  $\leq 1$  % by volume ilmenite. Assuming a 45 mg lunar sample is  
 660 collected into a ProSPA sized oven and contains 1 % ilmenite ( $\sim 0.45$  mg), a first order  
 661 estimate can be made for the amount of water produced. First, based on the data in  
 662 table 1, assume that the relationship between the amount of water produced and  
 663 condensed at the cold finger  $n_w$ , and the mass of ilmenite,  $m_{ilm}$ , is a second order  
 664 polynomial where  $n_w = -1 \times 10^{-5} m_{ilm}^2 + 9 \times 10^{-4} m_{ilm} + 0.0013$ . Assuming that the presence and  
 665 composition of other lunar minerals in the sample has no impact on the production of  
 666 water from the ilmenite present, then  $\sim 1.7$   $\mu\text{mol}$  of water (0.06 wt. % oxygen yield)  
 667 would be produced and condensed in 1 hour in the BDM system. A yield of this size  
 668 equates to a pressure in the BDM system of  $\sim 1.7$  mbar which is likely too small to be  
 669 identifiable above a blank reading. The presence of lunar minerals will also likely slow  
 670 down the movement of gases between grains, particularly if the ilmenite grains present

671 happen to be at the bottom of the sample or integrated into the matrix of other minerals  
672 in agglomerates. To improve these yields higher temperatures and longer reaction times  
673 would likely result in measurable yields. Also, other iron bearing lunar minerals can  
674 reduce including plagioclase and pyroxene, albeit at much lower efficiencies (Allen et  
675 al., 1994). As a result, low ilmenite concentrations may not be a barrier to the production  
676 and measurement of water from a lunar sample using a ProSPA-like system.

## 677 **6 Conclusions**

678 We have demonstrated that ilmenite can be reduced by hydrogen in a ProSPA-  
679 like static system operated at 900 °C for 1 hour, producing yields of up to  $1.4 \pm 0.1$  wt.%  
680 oxygen. Smaller samples react more fully, up to  $12.9 \pm 1.5$  % complete, as a result of the  
681 sample holder dimensions and reaction kinetics, as the reactants and products cannot  
682 easily move around the ilmenite grains. One of the implications of this work for ProSPA  
683 ISRU studies is the need for temperature control of the entire system if the extracted  
684 water is to be measured by its pressure in a closed system. This work has also  
685 highlighted the limitations of the current narrow/deep oven in a static (non-fluidized bed)  
686 configuration, currently estimating that there is a mass limit of ~30 mg (corresponding to  
687 a depth of ~2.3 mm) above which an increase in ilmenite mass does not result in an  
688 increase in water produced in the given time and at the given conditions. Although the  
689 system is not optimized for an ISRU reaction, it is a simple technique that can be used  
690 to perform a proof-of-principle reduction reaction of lunar ilmenite *in situ*.



691 **Acknowledgements**

692 The authors would like to acknowledge the support of Dr Giulia Degli-Alessandrini for  
693 assistance with operating the SEM, Dr Pallavi Anand for assistance with the Nikon  
694 SMZ1500 microscope and infinity capture software, and Dr Aiden Cowley for supplying  
695 the ilmenite used in the experiments. This work was supported by a Science and  
696 Technology Facilities Council (STFC) studentship grant [grant number ST/N50421X/1]  
697 to HS and by The Open University. ProSPA is being developed by a consortium led by  
698 The Open University, UK, under contract to the PROSPECT prime contractor Leonardo  
699 S.p.A., Italy, within a programme of and funded by the European Space Agency.

700 **References**

- 701 Allen, C. C., Morris, R. V., & McKay, D. S. (1994). Experimental reduction of lunar mare  
702 soil and volcanic glass. *Journal of Geophysical Research: Planets*, 99(E11), 23173-  
703 23185.
- 704 Altenberg, B., Franklin, H., & Jones, C. (1993). *Thermodynamics of lunar ilmenite*  
705 *reduction*. Paper presented at the Lunar and Planetary Science Conference XXIV,  
706 Houston, Texas.
- 707 Anand, M., Asher, Y., Buchwald, R., Carnelli, I., Carpenter, J., Conti, M., . . . Urbina, D.  
708 (2018). *Towards the use of lunar resources*. European Space Agency.
- 709 Barber, S., Smith, P., Wright, I., Abernethy, F., Anand, M., Dewar, K., . . . Morgan, G.  
710 (2017). *ProSPA: the Science Laboratory for the Processing and Analysis of Lunar Polar*  
711 *Volatiles within PROSPECT*. Paper presented at the 48th Lunar and Planetary Science,  
712 Houston, Texas.

- 713 Barber, S. J., Wright, I. P., Abernethy, F., Anand, M., Dewar, K. R., Hodges, M., . . .  
714 Trautner, R. (2018). *ProSPA: Analysis of Lunar Polar Volatiles and ISRU Demonstration*  
715 *on the Moon*. Paper presented at the 49th Lunar and Planetary Science Conference,  
716 Houston, Texas.
- 717 Buck, A. (1996). Buck Research CR-1A User's Manual. Buck Research Instruments:  
718 Boulder, CO, USA.
- 719 Chambers J. G., Taylor L. A., Patchen A., McKay D. S. (1995) Quantitative  
720 mineralogical characterization of lunar high-Ti mare basalts and soils for oxygen  
721 production. *Journal of Geophysical Research*, 100, 14391-14401.  
722 <https://doi.org/10.1029/95JE00503>
- 723 Christiansen, E., Simonds, C. H., & Fairchild, K. (1988). *Conceptual design of a lunar*  
724 *oxygen pilot plant*. LPI Contributions, 652, 52.
- 725 Dang, J., Zhang, G.-h., & Chou, K.-c. (2015). Kinetics and mechanism of hydrogen  
726 reduction of ilmenite powders. *Journal of Alloys and Compounds*, 619, 443-451.  
727 <https://doi.org/10.1016/j.jallcom.2014.09.057>
- 728 Delchar, T. A. (1993). *Vacuum physics and techniques*: Chapman and Hall.
- 729 Denk, T. (2018). *Full-Scale Terrestrial Demonstrator for ilmenite Reduction with*  
730 *Concentrated Solar Power*. Paper presented at the European Lunar Symposium,  
731 Toulouse, France.
- 732 ESA. (2018). *In-Situ Resource Utilisation (ISRU) demonstration mission*. Retrieved  
733 from [http://exploration.esa.int/moon/60127-in-situ-resource-utilisation-demonstration-](http://exploration.esa.int/moon/60127-in-situ-resource-utilisation-demonstration-mission/)  
734 [mission/](http://exploration.esa.int/moon/60127-in-situ-resource-utilisation-demonstration-mission/). Accessed 19/08/2019.

- 735 ESA. (2015). *Exploring Together: ESA Space Exploration Strategy*. Retrieved from  
736 Strategic Planning and Outreach Office of the ESA Directorate of Human Spaceflight  
737 and Operations, ESTEC, PO Box 299 2200 AG Noordwijk The Netherlands.
- 738 Geankoplis, C. J. (1993). *Transport Processes and Unit Operations*. (3 ed.). Engelwood  
739 Cliffs, NJ: PTR Prentice-Hall.
- 740 Gibson, M. A., & Knudsen, C. W. (1985). *Lunar oxygen production from ilmenite*. Paper  
741 presented at the Lunar bases and space activities of the 21st century, Houston, TX.
- 742 Goldstein, J. I., Newbury, D. E., Michael, J. R., Ritchie, N. W., Scott, J. H. J., & Joy, D.  
743 C. (2017). *Scanning electron microscopy and X-ray microanalysis*: Springer.
- 744 Hallis L. J., Anand M., Strekopytov S. (2014) Trace-element modelling of mare basalt  
745 parental melts: Implications for a heterogeneous lunar mantle. *Geochimica et*  
746 *Cosmochimica Acta*, (134) 289-316. <https://doi.org/10.1016/j.gca.2014.01.012>
- 747 ISECG, I. S. E. C. G. (Producer). (2018). *The Global Exploration Roadmap*. Retrieved  
748 from [https://www.nasa.gov/sites/default/files/atoms/files/ger\\_2018\\_small\\_mobile.pdf](https://www.nasa.gov/sites/default/files/atoms/files/ger_2018_small_mobile.pdf)
- 749 Linne, D., Kleinhenz, J., & Hegde, U. (2012). *Evaluation of Heat Recuperation in a*  
750 *Concentric Hydrogen Reduction Reactor*. Paper presented at the 50<sup>th</sup> AIAA Aerospace  
751 Sciences Meeting including the New Horizons Forum and Aerospace Exposition,  
752 Nashville, TN.
- 753 Linne, D. L., Gokoglu, S., Hegde, U. G., Balasubramaniam, R., & Santiago-Maldonado,  
754 E. (2009). *Component and System Sensitivity Considerations for Design of a Lunar*  
755 *ISRU Oxygen Production Plant*. Paper presented at the 47th AIAA Aerospace Sciences  
756 Meeting including The NewHorizons Forum and Aerospace Exposition, Orlando, FL.

- 757 Lomax, B., Conti, M., Khan, N., Ganin, A., & Symes, M. (2019). *The Metalysis-FCC-*  
758 *Cambridge process for efficient production of oxygen and metals on the lunar surface.*  
759 Paper presented at the European Lunar Symposium, Manchester, UK.
- 760 McKay, D. S., Heiken, G., Basu, A., Blanford, G., Simon, S., Reedy, R., . . . Papike, J.  
761 (1991). *The lunar regolith.* Lunar sourcebook, 285-356 (pg. 289)
- 762 Meyen, F. E., Hecht, M. H., & Hoffman, J. A. (2016). Thermodynamic model of Mars  
763 Oxygen ISRU Experiment (MOXIE). *Acta Astronautica*, 129, 82-87.  
764 doi:10.1016/j.actaastro.2016.06.005
- 765 Papike, Taylor, L., & S, S. (1991). *Lunar Minerals.* In G. Heiken, D. Vaniman, & B. M.  
766 French (Eds.), Lunar sourcebook (pp. 121-181).
- 767 Pfeiffer Vacuum, G. (2013). *Vacuum technology book* (Vol. II). Asslar, Germany: Pfeiffer  
768 Vacuum GmbH.
- 769 Rao, D. B., Choudary, U., Erstfeld, T., Williams, R. J., & Chang, Y. (1979). Extraction  
770 processes for the production of aluminum, titanium, iron, magnesium, and oxygen and  
771 nonterrestrial sources. In J. Billingham, W. Gilbreth, and B. O'Leary (Eds.) *Space*  
772 *Resources and Space Settlements* NASA SP-428, pp. 257-274.
- 773 Sanders G. B. & Larson, W. E. (2011). Integration of in-situ resource utilization into  
774 lunar/Mars exploration through field analogs. *Advances in Space Research*, 47(1), (20-  
775 29).
- 776 Sanders, G. B., & Larson, W. E. (2012). Progress made in lunar in situ resource  
777 utilization under NASA's exploration technology and development program. *Journal of*  
778 *Aerospace Engineering*, 26(1), 5-17.

- 779 Talboys, D., Barber, S., Bridges, J., Kelley, S., Pullan, D., Verchovsky, A., . . . Pillinger,  
780 C. (2009). In situ radiometric dating on Mars: Investigation of the feasibility of K-Ar  
781 dating using flight-type mass and X-ray spectrometers. *Planetary and Space Science*,  
782 57(11), 1237-1245.
- 783 Taylor, L., & Carrier, W. (1993). Oxygen Production on the Moon: An Overview and  
784 Evaluation. In J. S. Lewis, M. S. Matthews, & M. L. Guerrieri (Eds.), *Resources of Near-*  
785 *Earth Space* : University of Arizona Press pp. 69-108.
- 786 Taylor, L. A., Jerde, E. A., McKay, D. S., Gibson, M. A., Knudsen, C. W., & Kanamori,  
787 H. (1993). *Production of O<sub>2</sub> on the Moon: A lab-top demonstration of ilmenite reduction*  
788 *with hydrogen*. Paper presented at the Lunar and Planetary Science Conference XXIV,  
789 Houston, Texas.
- 790 Taylor, L. A., Pieters, C., Patchen, A., Taylor, D. H. S., Morris, R. V., Keller, L. P., &  
791 McKay, D. S. (2010). Mineralogical and chemical characterization of lunar highland  
792 soils: Insights into the space weathering of soils on airless bodies. *Journal of*  
793 *Geophysical Research: Planets*, 115(E2). <https://doi.org/10.1029/2009JE003427>
- 794 Trimble, J., & Carvalho, R. (2016). *Lunar prospecting: searching for volatiles at the*  
795 *south pole*. Paper presented at the 14<sup>th</sup> International Conference on Space Operations,  
796 Daejeon, Korea. <https://doi.org/10.2514/6.2016-2482>
- 797 Tuzi, Y., Tanaka, T., Takeuchi, K., & Saito, Y. (1996). Effect of surface treatment on the  
798 adsorption kinetics of water vapor in a vacuum chamber. *Vacuum*, 47(6-8), 705-708.
- 799 Warner R. D., Nehru C. E., Keil K. (1978) Opaque oxide mineral crystallization in lunar  
800 high-titanium mare basalts. *American Mineralogist* 63, 1209-1224.

- 801 Williams, R. J., McKay, D. S., Giles, D., & Bunch, T. E. (1979). Mining and beneficiation  
802 of lunar ores. In J. Billingham, W. Gilbreth, and B. O'Leary (Eds.) *Space Resources and*  
803 *Space Settlements* NASA SP-428, pp. 275-188.
- 804 Williams, R. J., & Mullins, O. (1983). *Enhanced production of water from ilmenite: An*  
805 *experimental test of a concept for producing lunar hydrogen*. Paper presented at the  
806 Lunar and Planetary Science XIV, Special Session Abstracts, Lunar and Planetary  
807 Institute, Houston.
- 808 Wright, I., Barber, S., Morgan, G., Morse, A., Sheridan, S., Andrews, D., . . . Leese, M.  
809 (2007). Ptolemy—an instrument to measure stable isotopic ratios of key volatiles on a  
810 cometary nucleus. *Space Science Reviews*, 128(1-4), 363-381.
- 811 Zhao, Y., & Shadman, F. (1993). Production of Oxygen from Lunar Ilmenite. In J. S.  
812 Lewis, M. S. Matthews, & M. L. Guerrieri (Eds.), *Resources of Near-Earth Space* (pp.  
813 149-178): University of Arizona Press.
- 814

Conflict of Interest statement

This work was supported by a Science and Technology Facilities Council (STFC) studentship grant [grant number ST/N50421X/1] to HS and by The Open University. ProSPA is being developed by a consortium led by The Open University, UK, under contract to the PROSPECT prime contractor Leonardo S.p.A., Italy, within a programme of and funded by the European Space Agency.

Journal Pre-proof